Revista Mexicana de Astronomía y Astrofísica, **54**, 1–20 (2018)

TESTING THE PLANET-METALLICITY CORRELATION IN M-DWARFS WITH GEMINI GNIRS SPECTRA

M. J. Hobson[1], E. Jofré[1,2], L. García[1], R. Petrucci,[1,2], and M. Gómez[1,2]

Received December 15 2016; accepted September 18 2017

ABSTRACT

While the planet-metallicity correlation for FGK main-sequence stars hosting giant planets is well established, it is less clear for M-dwarf stars. We determine stellar parameters and metallicities for 16 M-dwarf stars, 11 of which host planets, with near-infrared spectra from the Gemini Near-Infrared Spectrograph (GNIRS). We find that M-dwarfs with planets are preferentially metal-rich compared to those without planets. This result is supported by the analysis of a larger catalogue of 18 M stars with planets and 213 M stars without known planets (Terrien et al. 2015), and demonstrates the utility of GNIRS spectra to obtain reliable stellar parameters of M stars. We also find that M dwarfs with giant planets are preferentially more metallic than those with low-mass planets, in agreement with previous results for solar-type stars. These results favor the core accretion model of planetary formation.

RESUMEN

Mientras que la correlación planeta-metalicidad para las estrellas de secuencia principal FGK con planetas gigantes está bien establecida, los resultados no son claros para las enanas M. Se determinan parámetros estelares y metalicidades de 16 estrellas enanas M, incluyendo 11 con planetas, a partir de espectros infrarrojos de GNIRS (Gemini Near-Infrared Spectrograph). Se encuentra que las enanas M con planetas son preferentemente ricas en metales en comparación con aquellas sin planetas. Esto se confirma con el análisis de 18 estrellas M con planetas y 213 estrellas M sin planetas detectados (Terrien et al. 2015), y demuestra la utilidad de los espectros GNIRS. Las enanas M con planetas gigantes son preferentemente más metálicas que aquellas con planetas de menor masa, de acuerdo con lo reportado para estrellas de tipo solar. Estos resultados favorecen el modelo de acreción del núcleo de formación planetaria.

Key Words: methods: observational — planets and satellites: general — stars: abundances — techniques: spectroscopic

1. INTRODUCTION

M-dwarf stars are the greatest stellar component of the Galaxy, representing around 70% of stars (Kroupa et al. 2013). They are small, cool, faint stars, with masses ranging from $0.075M_{\odot}$ to $0.6M_{\odot}$, radii from $0.08R_{\odot}$ to $0.62R_{\odot}$, temperatures from 2100 K to 3800 K, and luminosities from $0.001L_{\odot}$ to $0.08L_{\odot}$ (Kaltenegger & Traub 2009). As the greatest stellar population, they may also represent the greatest population of planetary hosts (e.g. Lada 2006).

Nowadays it is widely accepted that FGK main-sequence and subgiant stars hosting gas giant planets are, on average, more metal-rich than stars without detected planets (e.g. Gonzalez 1997, Fischer & Valenti 2005, Ghezzi et al. 2010b). However, the existence of a planet-metallicity correlation is not so clear for stars hosting

[1]Observatorio Astronómico de Córdoba, Argentina.
[2]CONICET, Argentina.

Neptune-sized and smaller planets (e.g. Sousa et al. 2011, Mayor et al. 2011, Neves et al. 2013, Buchhave & Latham 2015, Wang & Fischer 2015). Moreover, the results for giant stars with planets have been ambiguous, and the issue is still debated (e.g. Maldonado et al. 2013, Jofré et al. 2015, Reffert et al. 2015).

There are two generally accepted models for planetary formation: gravitational instability and core accretion. In the gravitational instability model, dust particles settle into a thin disk with local overdense regions, which are unstable and undergo gravitational collapse. Successive collapses and collisions are responsible for the formation of planets (e.g. Goldreich & Ward 1973, Boss 1997, Youdin & Shu 2002). In the core accretion model, on the other hand, terrestrial planets and the solid cores of gas planets are formed by the accumulation of planetesimals. If a critical mass is reached before gas depletion, gas accretion from the disk begins and forms a giant planet (e.g. Pollack et al. 1996, Mordasini et al. 2009).

The planet-metallicity correlation found for main-sequence FGK stars would provide support for the core accretion planet formation scenario. A more metallic environment allows the rapid formation of planetary cores which can start to accrete gas from the surrounding disk to form gas giant planets (Pollack et al. 1996), whereas in low-metallicity the cores form too slowly for accretion to take place before the disk is depleted (Ida & Lin 2004, Mayor et al. 2011, Mordasini et al. 2012). The considerably low metallicity ([Fe/H] ≈ -0.30 dex, e.g. Santos et al. 2010) of several main-sequence (MS) stars hosting giant planets, and the average low metallicity found for giant stars with planets (≈ -0.08 dex; Jofré et al. 2015) raises the issue of giant planet formation within the framework of the metallicity-dependent core accretion model. Johnson & Li (2012) derived the minimum metallicity function required for planet formation in the core accretion scenario, and found that none of the ≈ 320 planet-hosting stars reported by 2011 were below the critical metallicity. Similar results are found for evolved stars with planets (Jofré et al. 2015). On the other hand, it has been suggested that the more massive disks around higher-mass stars, such as evolved stars with planets[3], would compensate their lower metallic abundances and hence enable giant-planet formation (Ghezzi et al. 2010a, Maldonado et al. 2013). The situation for the formation of giant planets around M-dwarfs may be even less clear, since theoretical predictions within the core accretion model foresee that the giant-planet-formation may be inhibited at all radial distances (Laughlin et al. 2004).

Given the role that stellar properties, such as metallicity and mass, may play in the process of planet formation, it is also important to confirm (or refute) the planet-metallicity correlation results for stars at the lower end of the mass scale, such as M dwarfs. However, while for FGK stars metallicities can be determined with great accuracy using high-resolution spectra ($R \gtrsim 30000$) in the optical range, the spectra of M-dwarf stars are extremely complex, with many blended lines and strong molecular bands (e.g., TiO, VO) preventing an easy continuum fit and thus complicating a precise metallicity determination. While some studies (e.g., Bean et al. 2006, Woolf & Wallerstein 2006) have attempted determinations using high-resolution optical spectra, they have been limited to few and/or metal-poor stars. Önehag et al. (2012) adopted a slightly different approach, using high-resolution spectra ($R = 50000$) in the infrared J band; this spectral region has few molecular components, enabling precise continuum and line fitting. The need for high resolution, however, limits this technique, as bright stars and/or long integration times are necessary. Additionally, M dwarfs are typically brighter in the H and K bands than in the J band.

Wide-band photometric calibrations using $V - K$ and M_K were performed for M-dwarfs by Bonfils et al. (2005a), Johnson & Apps (2009), and Schlaufman & Laughlin (2010), with conflicting results: Johnson & Apps (2009) found that only Jupiter hosts are metal-rich, while Schlaufman & Laughlin (2010) reported that both Jupiter and Neptune hosts are metal-rich. For Jupiter hosts, both results are therefore in agreement with that found for FGK stars, whereas the situation for Neptune hosts is not clear for either FGK stars or M-dwarfs. Bonfils et al. (2005a) studied only two planetary hosts, Gl 876 and Gl 436, finding near-solar metallicities for both. Additionally, Schlaufman & Laughlin (2010) noted that Bonfils et al. (2005a) systematically underestimated metallicities, while Johnson & Apps (2009) overestimated them. The main disadvantage of these photometric techniques is the need for absolute magnitudes; their determination requires accurate stellar distances, which limits the stars to which these techniques can be applied. However, it is expected that the ongoing ESA astrometric mission, Gaia (Gaia Collaboration et al. 2016) will provide accurate distances for all

[3]Giants with planets usually have masses between 0.9 and 4 $M_\odot$ (e.g., Sato et al. 2005, Niedzielski et al. 2007, Jofré et al. 2015, Ghezzi & Johnson 2015).

objects down to G $\approx$ 20 mag [4], and therefore the number of M stars whose metallicities could be determined by the photometric techniques would be significantly increased.

Recently, a new technique for determining the metallicities of M dwarfs via near infrared (NIR) spectra was developed by Rojas-Ayala et al. (2010) and Terrien et al. (2012). This technique requires only moderate-resolution NIR spectra to reliably estimate metallicities, which greatly reduces the observing time required. Additionally, it is not limited to nearby stars with known parallaxes. It is calibrated using wide FGK-M binaries: assuming a common origin, and therefore a common metallicity, for both stars, the metallicity of the FGK component is measured using high-resolution spectroscopy and assigned to the M-dwarf companion. Linear regressions are then performed between these metallicities and the equivalent widths (EWs) of the selected NIR spectral features, resulting in a best-fit relationship between the EWs and the metallicity. Using this technique, Rojas-Ayala et al. (2012) found an apparent planet-metallicity correlation over 133 M dwarfs including 11 planet hosts, which is strongest for Hot Jupiters, using spectra from the TripleSpec spectrograph on the Palomar 200-inch Hale Telescope with $R \approx 2700$. Likewise, Terrien et al. (2012) found that five giant planet hosts are more metal-rich than four M-dwarf planet hosts without known giant planets, using spectra from the NASA-Infrared Telescope Facility SpeX Spectrograph with $R \approx 2000$ [5].

Gaidos & Mann (2014) used JHK spectra to derive metallicities of 121 M dwarfs and study the occurrence of giant planet dependence on metallicity for both M-dwarfs and solar-type stars. Their results hint to a deficiency of giant planets in M dwarfs, although this deficiency is not very significant. More recently, Gaidos et al. (2016), using a photometric calibration in $J - H$, obtained metallicities for M dwarfs and found that the distribution in metallicity of M dwarfs with planets (usually small planets) is indistinguishable from that of M dwarfs without known planets. Souto et al. (2017), using high-resolution ($R \approx 22,500$) H-band spectra from the SDSS-IV-APOGEE survey, derived chemical abundances for 13 elements for two M-dwarfs with multiplanetary systems, Kepler 138 and Kepler 186, and obtained sub-solar metallicities. They found, however, that in both cases previous metallicity determinations from lower-resolution spectra were sub-estimated by 0.1– 0.2 dex.

Taking into account the lack of consensus about the planet-metallicity correlation in M dwarf stars, in this work we applied the techniques developed in the NIR to homogeneously determine stellar parameters and metallicities of 16 M dwarfs (11 of which have planets) from spectra obtained with the Gemini North Near-Infrared Spectrograph (GNIRS). In § 2 we present the observations and data reduction; in § 3 the determinations of the stellar parameters, including metallicity; searches for correlations between metallicity and planetary parameters are presented in § 4. To test if trends suggested by GNIRS spectra are also supported by relatively larger samples, we used two subsamples of M dwarfs with and without known planets from the catalogue of Terrien et al. (2015). Finally in § 5 we summarize the conclusions.

2. OBSERVATIONS AND DATA REDUCTION

NIR spectra were obtained for a sample of 11 M dwarfs with planets and 5 without known planets using the GNIRS spectrograph, mounted on the Gemini North telescope. The observations were carried out during the 2012B and 2013A semesters (programs GN-2012B-Q-23 and GN-2013A-Q-66 respectively). In the 2012B program, five stars were observed: GJ 176, GJ 179, GJ 250 B, GJ 297.2 B, and GJ 317. The remaining 11 stars (GJ 436, GJ 581, GJ 611 B, GJ 649, GJ 777 B, GJ 783.2 B, GJ 849, GJ 876, GJ 1214, HIP 57050, and HIP 79431) were observed in the 2013A program. The spectrograph was used in cross-dispersed mode, covering a range of $1.2 - 2.5$ μm, with $R \approx 1700$; to achieve this, the 10.5 l/mm grating, long blue camera (0.05 arcsec/pix) plus the SXD prism and a 0.45 arcsec slit were employed. Table 1 lists the M-stars observed, the V and K magnitudes, the corresponding telluric standard stars, and the number of planets and discovery papers, where applicable.

The spectra were reduced using the XDGNIRS pipeline developed by Rachel Mason and Omaira González-Martín[6]. This pipeline creates and subtracts the flatfield, removes electronic pattern noise, cuts and straightens the orders, wavelength calibrates, extracts the spectrum, removes telluric lines (based on a telluric standard, listed in Table 1 for each star), flux calibrates, and calculates the SNR of the spectrum. Finally, the reduced

[4] G represents the broad-band, white-light, Gaia magnitude with wavelength coverage 330-1050 nm.

[5] We note that H- and/or K-band spectra have not only been applied to derive metallicities of M dwarfs with planets, but also of late-type stars in the Kepler field (Muirhead et al. 2014), of nearby M-dwarfs (Newton et al. 2014) and of mid- and late-M dwarfs (Mann et al. 2015), in general.

[6] Obtained from `http://drforum.gemini.edu/wp-content/uploads/2013/11/XDGNIRS_v20.pdf`

TABLE 1

OBSERVED M-STARS WITH AND WITHOUT PLANETS

Star	$V^{\dagger}$	$K^{\dagger}$	SNR‡	Telluric Standard	Planets	Reference
GJ 1214	14.67	8.782	101	HIP 87108	1	1
GJ 176	9.951	5.607	85	HIP 22913	1	2
GJ 179	12.018	6.942	95	HIP 22913	1	3
GJ 317	11.975	7.028	83	HIP 43269	2	4
GJ 436	10.613	6.073	40	HIP 57014	1	5
GJ 581	10.560	5.837	91	HIP 73249	3	6, 7, 8
GJ 649	9.655	5.624	86	HIP 85790	2	9, 10
GJ 849	10.366	5.594	86	HIP 109442	2	11, 12
GJ 876	10.192	5.010	96	HIP 115119	4	13, 14, 15, 16
HIP 57050	11.959	6.822	82	HIP 57014	1	17
HIP 79431	11.372	6.589	64	HIP 79124	1	18
Star	$V^{\dagger}$	$K^{\dagger}$	SNR‡	Telluric Standard		
GJ 250 B	10.05	5.72	42	HIP 33420		
GJ 297.2 B	11.815	7.418	52	HIP 42444		
GJ 611 B	14.206	9.159	82	HIP 78649		
GJ 777 B	14.40	8.712	76	HIP 98699		
GJ 783.2 B	13.932	8.883	67	HIP 99742		

†Obtained from SIMBAD, `http://simbad.u-strasbg.fr/simbad/` (Wenger et al. 2000).

‡SNR for the $2.1 - 2.2$ μm region.

References: (1) Charbonneau et al. (2009); (2) Endl et al. (2008); (3) Howard et al. (2010); (4) Johnson et al. (2007); (5) Butler et al. (2004); (6) Bonfils et al. (2005b); (7) Udry et al. (2007); (8) Mayor et al. (2009); (9) Johnson et al. (2010); (10) Wittenmyer et al. (2013); (11) Butler et al. (2006); (12) Montet et al. (2014); (13) Delfosse et al. (1998); (14) Marcy et al. (2001); (15) Rivera et al. (2005); (16) Rivera et al. (2010); (17) Haghighipour et al. (2010); (18) Apps et al. (2010).

spectra were normalised using standard IRAF[7] tasks. The signal-to-noise ratios (SNR) in the observed spectra for the $2.1 - 2.2$ μm region (calculated as mean/rms of the normalised spectra in the region) are listed in Table 1. Figures 1 and 2 show the normalised spectra in the H and K bands respectively. The targets in our sample have radial velocities < 100 kms^{-1}, so any spectral-feature-wavelength displacement would be $\lesssim 10^{-3}$ μm, and thus indistinguishable within our resolution.

3. ANALYSIS

3.1. *Fundamental Stellar Parameters*

In this section we use our GNIRS/Gemini spectra and the calibrations from Newton et al. (2015) to calculate temperatures, radii, and Log L of the stars in our sample and compare them with previous estimations from the literature. The aim is to verify whether GNIRS/Gemini spectra are suitable to derive fundamental stellar parameters.

Calibrations from Newton et al. (2015) make use of the equivalent widths (EWs) of the Al doublet at 1.67 μm and three Mg lines at 1.50, 1.57, and 1.71 μm in the H band. For details about the precise feature

[7]IRAF is distributed by the National Optical Astronomy Observatories, which are operated by the Association of Universities for Research in Astronomy, Inc., under cooperative agreement with the National Science Foundation.

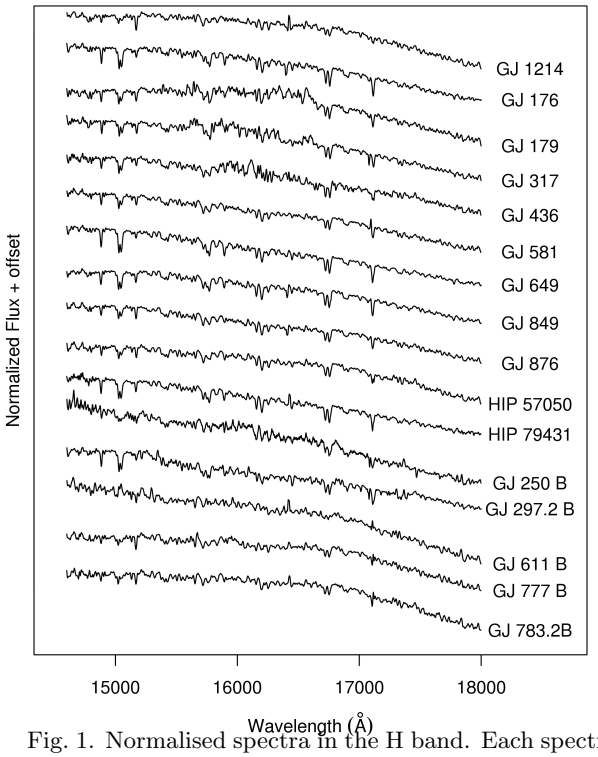

Fig. 1. Normalised spectra in the H band. Each spectrum has been normalised by its mean flux between 1.46 and 1.80 μm and arbitrarily shifted.

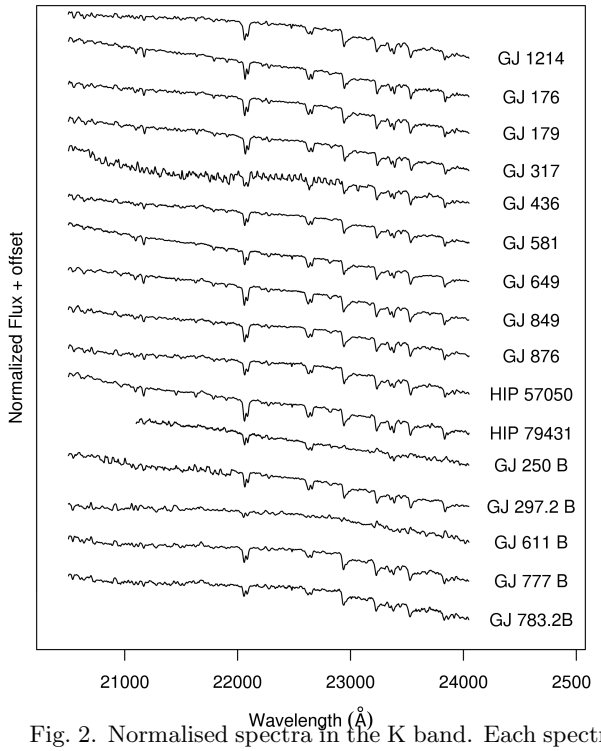

Fig. 2. Normalised spectra in the K band. Each spectrum has been normalised by its mean flux between 2.05 and 2.405 μm and arbitrarily shifted.

windows and regions used to estimate the continuum for each line, we refer the reader to Table 1 of Newton et al. (2015). The EWs[8] were calculated from the standard definition:

$$EW_\lambda = \sum_i \left[1 - \frac{I(\lambda_i)}{I_c(\lambda_i)}\right] \Delta\lambda_i, \quad (1)$$

with i the pixels spanned by the line, λ_i the wavelength at pixel i, $I(\lambda_i)$ the observed line intensity at pixel i, $I_c(\lambda_i)$ the calculated continuum intensity at pixel i, and $\Delta\lambda_i$ the pixel width. The continuum for each line was defined, in accordance with Newton et al. (2015), as a linear fit to the corresponding blue and red continuum regions. Once the EWs were measured, we calculated the stellar parameters using the expresions:

$$T_{\rm eff}/K = 271.4 \times EW_{Al\text{-}a(1.67\mu m)} + 392.7 \times EW_{Mg(1.50\mu m)}/EW_{Al\text{-}b(1.67\mu m)} + 2427 \quad (2)$$

$$R/R_\odot = -0.0489 \times EW_{Mg(1.57\mu m)} + 0.275 \times EW_{Al\text{-}a(1.67\mu m)} + 0.201 \times EW_{Mg(1.57\mu m)}/EW_{Al\text{-}a(1.67\mu m)} - 0.216 \quad (3)$$

$$\log L/L_\odot = 0.832 \times EW_{Mg(1.71\mu m)} - 0.176 \times [EW^2_{Mg(1.71\mu m)}] + 0.266 \times EW_{Mg(1.50\mu m)} - 3.491, \quad (4)$$

with EW_X the equivalent width measured for element X.

The results are reported in Table 2. The errors were estimated using Monte Carlo methods: random Gaussian noise based on the SNR was added to each spectrum, and the EWs were recalculated. We performed this 100 times for each target, and estimated the EW errors as the standard deviation of the 100 runs. The errors of the parameters were then obtained by propagation in quadrature. All the stellar parameters of GJ

[8]For all EWs measured in this work, we visually verified that spectral features were included in the defined windows in spite of any (modest) shifts due to stellar radial velocities.

TABLE 2

STELLAR PARAMETERS DERIVED IN THIS WORK FOR THE OBSERVED M-STARS

Star	Temperature [K]	Radius [$R_\odot$]	log L [$L_\odot$]
GJ 176	3531 ± 50	0.44 ± 0.04	-1.48 ± 0.11
GJ 179	3362 ± 49	0.40 ± 0.03	-1.94 ± 0.11
GJ 250 B	†	†	-2.26 ± 0.22
GJ 297.2 B	3553 ± 114	0.37 ± 0.07	-1.54 ± 0.21
GJ 317	3234 ± 45	0.41 ± 0.04	-2.02 ± 0.11
GJ 436	3603 ± 182	0.31 ± 0.08	-1.89 ± 0.20
GJ 581	3357 ± 57	0.30 ± 0.04	-2.06 ± 0.10
GJ 649	3695 ± 51	0.46 ± 0.03	-1.32 ± 0.13
GJ 777 B	†	0.23 ± 0.05	†
GJ 783.2 B	†	0.23 ± 0.06	†
GJ 849	3408 ± 45	0.41 ± 0.04	-1.60 ± 0.13
GJ 876	3285 ± 48	0.29 ± 0.04	-2.10 ± 0.10
HIP 57050	3295 ± 50	0.30 ± 0.03	-2.15 ± 0.10
HIP 79431	3391 ± 52	0.42 ± 0.04	-1.64 ± 0.15

†Parameter outside the ranges in which Newton et al. (2015)'s calibrations are valid.

611 B and GJ 1214 were outside the ranges in which Newton et al. (2015)'s calibrations are valid, so those objects were omitted from the table. Additionally, for other stars only some of the parameters were outside these ranges; for these stars, we report only the parameters with the ranges of validity.

For the temperatures we found average differences of 13, 34, and 20 K with the estimations from Mann et al. (2013), Terrien et al. (2015), and Newton et al. (2015), respectively. These differences are within the uncertainties of our temperatures. With Rojas-Ayala et al. (2012) we found an average difference of ≈ 100 K. We point out that this comparison is only possible for 8 and 5 stars in the case of Mann et al. (2013) and Newton et al. (2015), respectively. With regard to Rojas-Ayala et al. (2012) and Terrien et al. (2015) we have 11 stars in common for which temperatures are provided.

The comparison of radii and luminosities is rather limited due to the small number of objects. However, for the 5 stars (GJ 176, GJ 436, GJ 581, GJ 649, and GJ 876) we have in common with Newton et al. (2015), we found a reasonably good agreement with an average difference of 0.05 $R_\odot$, which is of the same order as the errors in our determinations. A similar result was found for $\log L$ with an average difference of 0.1 $L_\odot$. Terrien et al. (2015) provide radii for 13 stars in common with our sample. Our determinations agree with thier published values, with an average difference of 0.02 $R_\odot$. Unfortunaltely, no individual values of radius and luminosity are reported in the other works cited above.

To explore the existence of any systematic difference that might be masked in the determination of the final values of temperatures, radii and luminosities, we directly compared our measured EWs for Al-a, Al-b, Mg(1.5 μm), Mg(1.57 μm), and Mg(1.71 μm) with those from the literature. As mentioned above we have only 5 stars in common with Newton et al. (2015) which prevents a detailed analysis, and 16 stars with Terrien et al. (2015). However, we found a good agreement in both cases, suggesting an absence of systematic differences in the EWs measured from GNIRS spectra with respect to previous determinations. A more thorough comparison to definitely rule out any difference would require a larger common sample.

3.2. *Stellar Metallicities*

To estimate the stellar metallicities, we used the calibrations developed by Rojas-Ayala et al. (2010), which were updated in Rojas-Ayala et al. (2012), those determined by Terrien et al. (2012), and those developed by Mann et al. (2013). While all these calibrations are based on moderate-resolution NIR spectra, there are differences between them: Rojas-Ayala et al. (2012) only use lines from the K-band - Na I doublet ($\lambda = 2.206$

and $\lambda = 2.2069\ \mu m$) and Ca I triplet ($\lambda = 2.261$, $\lambda = 2.263$, and $\lambda = 2.265\ \mu m$) - and define the continuum via linear fits to regions close to each line. Terrien et al. (2012) give calibrations for both the K-band - Na ($\lambda = 2.2074\ \mu m$) and Ca ($\lambda = 2.2638\ \mu m$) lines - and the H band - Ca ($\lambda = 1.6159$ and $\lambda = 1.6203\ \mu m$) and K ($\lambda = 1.5171\ \mu m$) lines, and define a continuum for the whole of each band using fourth-order Legendre polynomials. Finally, Mann et al. (2013) select regions empirically determined to be sensitive to metallicity changes in the H, J, and K bands, and define the continuum by linear fits over regions close to each line. The precise feature windows for each line and the regions used to define the continuum can be consulted in the corresponding works. As an example, Figure 3 shows the spectral lines employed for each calibration and the regions used to define the continuums for GJ 1214.

For all calibrations, the EWs were calculated by definition using Eq. 1. The fourth-order Legendre polynomial continuum fits for Terrien et al. (2012)'s calibration were performed using the IRAF *splot* task, whereas the linear continuum fits for Rojas-Ayala et al. (2012)'s and Mann et al. (2013)'s calibrations were carried out with least-square regression methods.

In addition to the EWs of the spectral lines, all calibrations also use H_2O indices in their metallicity determinations to account for the effects of stellar temperature. These indices are given by:

$$H_2O\text{-}K_{RA} = \frac{\langle F(2.070 - 2.090)\rangle / \langle F(2.235 - 2.255)\rangle}{\langle F(2.235 - 2.255)\rangle / \langle F(2.360 - 2.380)\rangle} \tag{5}$$

(Rojas-Ayala et al. 2012) and

$$\begin{aligned} H_2O\text{-}K_T &= \frac{\langle F(2.180 - 2.200)\rangle / \langle F(2.270 - 2.290)\rangle}{\langle F(2.270 - 2.290)\rangle / \langle F(2.360 - 2.380)\rangle} \\ H_2O\text{-}H_T &= \frac{\langle F(1.595 - 1.615)\rangle / \langle F(1.680 - 1.700)\rangle}{\langle F(1.680 - 1.700)\rangle / \langle F(1.760 - 1.780)\rangle} \end{aligned} \tag{6}$$

(Terrien et al. 2012), with $\langle F(a-b)\rangle$ the mean flux in the range defined by a and b (in μm). Mann et al. (2013) employed Terrien et al. (2012)'s H-band index and Rojas-Ayala et al. (2012)'s K-band index. The final calibration equations are:

$$[Fe/H]_{RA} = -1.039 + 0.092 \times EW_{Na}/H_2O\text{-}K + 0.119 \times EW_{Ca}/H_2O\text{-}K \tag{7}$$

(Rojas-Ayala et al. 2012)

$$\begin{aligned} [Fe/H]_{T,Kband} =& 0.132 \times EW_{Na} + 0.083 \times EW_{Ca} - 0.403 \times H_2O\text{-}K - 0.616 \\ [Fe/H]_{T,Hband} =& 0.340 \times EW_{Ca} + 0.407 \times EW_K + 0.436 \times H_2O\text{-}H - 1.485 \end{aligned} \tag{8}$$

(Terrien et al. 2012), and

$$\begin{aligned} [Fe/H]_{M,Kband} =& 0.19 \times EW_{F19} + 0.069 \times EW_{F22} + 0.083 \times EW_{F20} + 0.218 \times H_2O\text{-}K - 1.55 \\ [Fe/H]_{M,Hband} =& 0.40 \times EW_{F17} + 0.51 \times EW_{F14} - 0.28 \times EW_{F18} - 1.460 \times H_2O\text{-}H + 0.71 \end{aligned} \tag{9}$$

(Mann et al. 2013).

Table 3 presents the metallicities obtained by each method. Both the errors of the EWs, and the quoted uncertainties of the calibrations employed, are sources of uncertainty in the metallicity determinations. Taking a conservative approach, we chose to adopt for the metallicity error the largest value between that obtained by propagating the EWs and H_2O indices errors, and the quoted uncertainty of the calibration employed (0.14 for Rojas-Ayala et al. 2012, 0.12 for Terrien et al. 2012, 0.07 for Mann et al. 2013 in the H band, and 0.06 for Mann et al. 2013 in the K band), in each case.

The errors for the EWs and H_2O indices required by Rojas-Ayala et al. (2012)'s and Mann et al. (2013)'s calibrations were estimated using Monte Carlo methods: random Gaussian noise based on the SNR was added to each spectrum, and the EWs and H_2O indices were recalculated. We performed this 1000 times for each target, and estimated the EWs and H_2O indices errors as the standard deviation of the 1000 runs. For Terrien et al. (2012)'s calibration, the more elaborate continuum fit made Monte Carlo error estimations too complex.

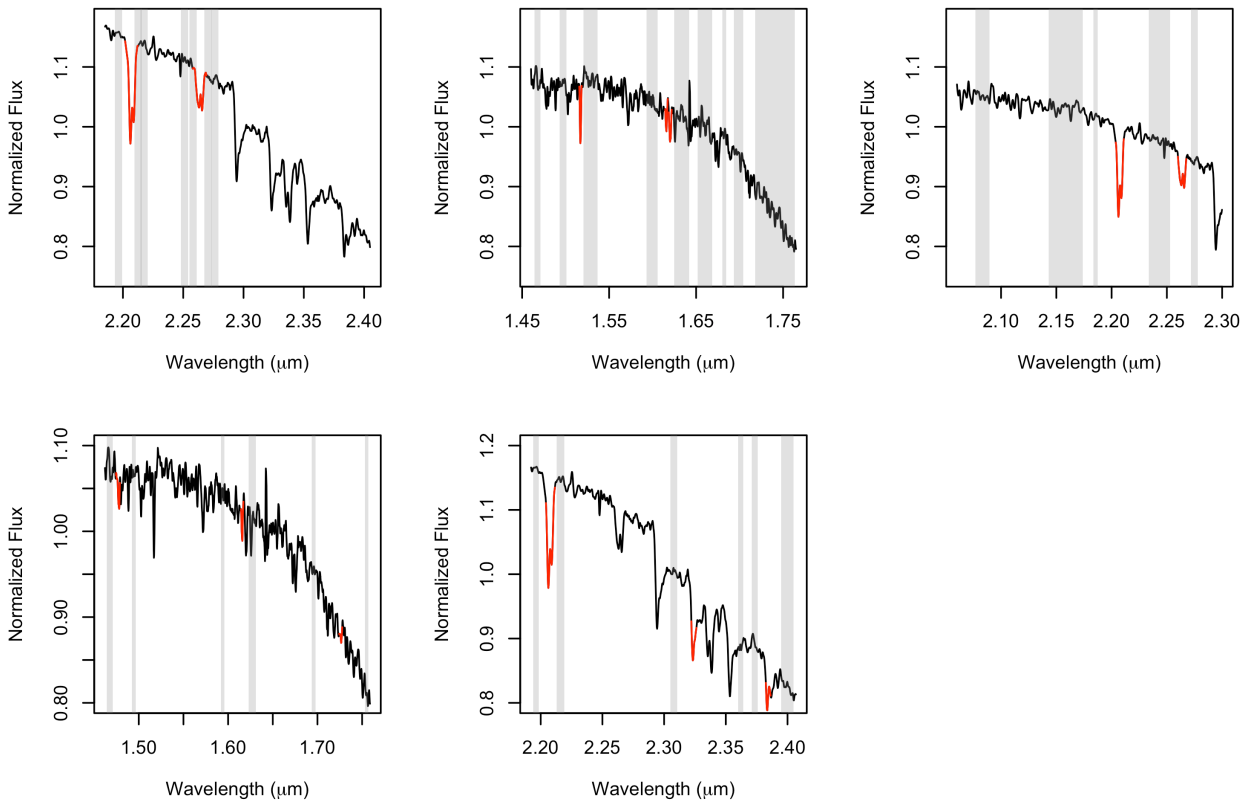

Fig. 3. Continuum regions (grey rectangles) and spectral lines (red continuous lines) used to determine metallicity for GJ 1214 following: top panels from left to right, Rojas-Ayala et al. (2012)'s method, Terrien et al. (2012)'s method in the H band, and Terrien et al. (2012)'s method in the K band; bottom panels from left to right, Mann et al. (2013)'s method in the H and in the K bands, respectively. Each spectrum has been normalised by the mean flux in the shown spectral region. The color figure can be viewed online.

Therefore, we used an analytic method developed by Sembach & Savage (1992), which was also employed by Terrien et al. (2012). Two stars in Table 3, GJ 250 B and GJ 611 B, show different metallicity values depending on calibrations or spectral bands used. Our spectrum for GJ 250 B has relatively lower SNR in comparison with the rest of the stars in Table 3 (see Table 1). In the case of GJ 611 B, it was not possible to achieve completely satisfactory telluric correction, resulting in a relatively noisy spectrum. These facts may explain the differences shown in Table 3.

The calibrations of Rojas-Ayala et al. (2012) and Terrien et al. (2012) are based on ≈ 20 wide binary stars and are valid for M0–M4 dwarfs and near solar metallicities ($-0.4 \lesssim$ [Fe/H] $\lesssim +0.3$). Using a larger number of calibrators (110 wide binaries), Mann et al. (2013) refined these calibrations and expanded the limits of validity in metallicity ($-1.04 <$ [Fe/H] $< +0.56$) and ranges of spectral types (K5–M6). For all bands, including the J-band, Mann et al. (2013) found it possible to obtain reliable metallicities (<0.10 dex), although features in the K-band provide the best results.

Recently, Terrien et al. (2015) applied the calibrations of Mann et al. (2013) to a large sample of M dwarfs and compared the results with the ones obtained from other similar calibrations such as the ones of Terrien et al. (2012), Mann et al. (2014), and Newton et al. (2014), all of which were developed with data from the same instrument (IRTF-SpeX, $R \approx 2000$). Finally, they chose the K-band-calibration derived metallicities of Mann et al. (2013) as the preferred measure of [Fe/H] for M1–M5 dwarfs. This calibration is not only based on a larger number of calibrators and has a wider spectral range of validity, but also provides a better agreement with other literature measurements and stability against small radial velocity shifts.

TABLE 3

STELLAR METALLICITIES DERIVED IN THIS WORK

Star	$[Fe/H]_{RA12}$[1]	$[Fe/H]_{T12,(K-band)}$[2]	$[Fe/H]_{T12,(H-band)}$[3]	$[Fe/H]_{M13,(K-band)}$[4]	$[Fe/H]_{M13,(H-band)}$[5]
GJ 176	0.008 ± 0.14	0.08 ± 0.12	0.17 ± 0.13	0.17 ± 0.06	-0.07 ± 0.09
GJ 179	0.06 ± 0.14	0.17 ± 0.12	0.36 ± 0.19	0.26 ± 0.06	0.04 ± 0.08
GJ 250 B	-0.34 ± 0.14	-0.29 ± 0.14	-0.004 ± 0.19	-0.79 ± 0.08	-0.29 ± 0.19
GJ 297.2 B	-0.07 ± 0.14	-0.10 ± 0.12	-0.17 ± 0.16	0.00 ± 0.06	-0.40 ± 0.15
GJ 317	0.08 ± 0.14	0.24 ± 0.12	0.21 ± 0.21	0.25 ± 0.06	-0.08 ± 0.09
GJ 436	-0.23 ± 0.14	-0.20 ± 0.12	-0.78 ± 0.19	-0.21 ± 0.08	-0.38 ± 0.19
GJ 581	-0.15 ± 0.14	-0.01 ± 0.12	-0.057 ± 0.12	-0.07 ± 0.06	-0.22 ± 0.09
GJ 611 B	-0.78 ± 0.14	†	†	-1.20 ± 0.06	-0.93 ± 0.10
GJ 649	-0.05 ± 0.14	0.01 ± 0.12	0.11 ± 0.12	0.00 ± 0.06	-0.15 ± 0.09
GJ 777 B	-0.17 ± 0.14	-0.04 ± 0.12	-0.006 ± 0.16	0.03 ± 0.06	0.07 ± 0.11
GJ 783.2 B	-0.36 ± 0.14	-0.15 ± 0.12	-0.21 ± 0.16	-0.25 ± 0.07	-0.32 ± 0.13
GJ 849	0.19 ± 0.14	0.31 ± 0.12	0.43 ± 0.13	0.44 ± 0.06	0.12 ± 0.09
GJ 876	0.09 ± 0.14	0.22 ± 0.12	0.10 ± 0.13	0.32 ± 0.06	0.01 ± 0.08
GJ 1214	-0.008 ± 0.14	0.19 ± 0.12	0.11 ± 0.12	0.41 ± 0.06	-0.22 ± 0.08
HIP 57050	-0.09 ± 0.14	0.02 ± 0.12	-0.04 ± 0.14	0.05 ± 0.06	-0.15 ± 0.12
HIP 79431	0.37 ± 0.14	0.58 ± 0.12	0.20 ± 0.12	0.66 ± 0.05	0.20 ± 0.12

[1]Metallicities obtained following Rojas-Ayala et al. (2012).

[2]Metallicities obtained following Terrien et al. (2012) for the K band.

[3]Metallicities obtained following Terrien et al. (2012) for the H band.

[4]Metallicities obtaine d following Mann et al. (2013) for the K band.

[5]Metallicities obtained following Mann et al. (2013) for the H band.

†Terrien et al. (2012)'s methods could not be applied to this star because the spectra were too noisy to allow for the fitting of the Legendre polynomial continuums.

3.3. *Comparison with the Literature and Selected Calibration*

In order to check the consistency of our results with previous estimations, we compared the [Fe/H] of the stars we have in common with Rojas-Ayala et al. (2012), Terrien et al. (2012), and Terrien et al. (2015). Unfortunately, Mann et al. (2013) do not provide metallicities with their calibrations. Figure 4 shows the comparison of our [Fe/H] values based on K-band calibrations to those from Rojas-Ayala et al. (2012), Terrien et al. (2012), and Terrien et al. (2015), along with the median offset (Δ[9]) and the standard deviation (σ) of the differences. We found that our estimated [Fe/H] are, in general, smaller than the [Fe/H] listed by Rojas-Ayala et al. (2012). On the other hand, our measured [Fe/H] show very good agreement with those derived by Terrien et al. (2012). In the case of the comparison with Terrien et al. (2015), there are two stars (GJ 250 B and GJ 611 B) for which the [Fe/H] we measure deviate considerably and systematically from the values obtained by these authors. As noted in § 3.2 this may be attributed to the relatively low quality of our spectra for these stars.

Analogously, Figure 5 shows the comparison of our [Fe/H] values based on H-band calibrations with those from Terrien et al. (2012) and Terrien et al. (2015). Our measured [Fe/H] values are consistent with those of Terrien et al. (2012) within error bars, with exception of GJ 436, for which our spectra has relatively low SNR (see Table 1). Our determinations are in general ≈ 0.16 dex lower than those presented by Terrien et al. (2015). In both cases, as has been previously reported by Mann et al. (2013) and Terrien et al. (2015), it can be seen that the results using H-band calibrations show significantly larger scatter than the ones obtained from K-band calibrations.

We also compared EWs and H_2O indices when possible. For Rojas-Ayala et al. (2012) we found that our EWs for Na and Ca are, in general, smaller for 13 stars. The average difference is of $\approx 10\%$. For Terrien et al.

[9]With Δ defined as the median difference between our determinations and the literature values.

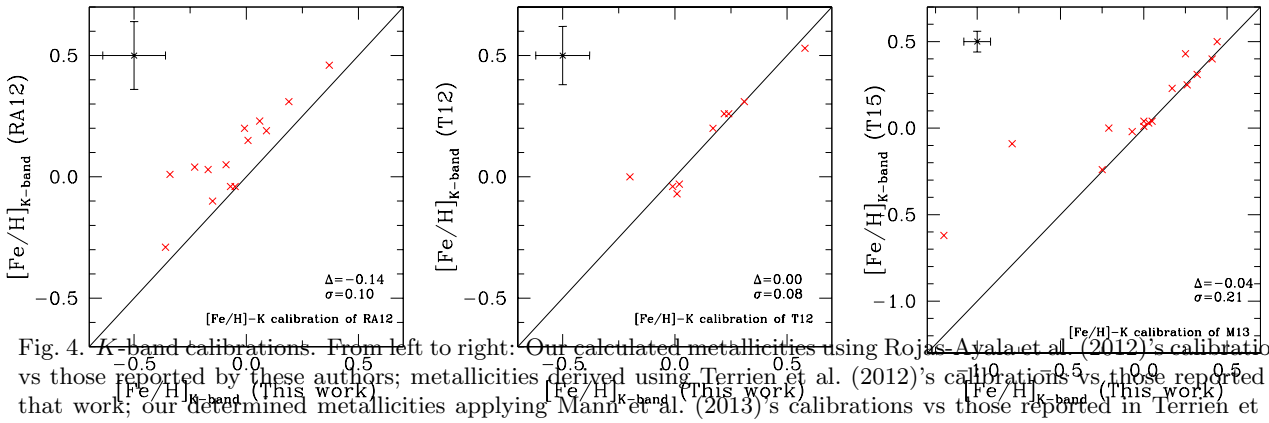

Fig. 4. *K*-band calibrations. From left to right: Our calculated metallicities using Rojas-Ayala et al. (2012)'s calibrations vs those reported by these authors; metallicities derived using Terrien et al. (2012)'s calibrations vs those reported in that work; our determined metallicities applying Mann et al. (2013)'s calibrations vs those reported in Terrien et al. (2015). The black continuous lines correspond to the identity. In the case of the Rojas-Ayala et al. (2012)'s calibration our metallicities are systematically lower than those from the literature. On the other hand the comparison with Terrien et al. (2012) shows that the metallicities are equivalent within error bars. With regard to Terrien et al. (2015), we find a good agreement, except for two stars (GJ 250 B and GJ 611 B) with relatively low quality GNIRS spectra.

(2012) the comparison for 4 stars (GJ 250 B, GJ 297.2 B, GJ 777 B, and GJ 783.2 B) shows a better agreement with our measured EWs with an average difference of $\approx 5\%$. No equivalent widths are given in Terrien et al. (2015). Comparisons of H_2O indices were possible only with those of Rojas-Ayala et al. (2012). In general, our calculated H_2O indices are larger than those reported by Rojas-Ayala et al. (2012) with an average difference of $\approx 8\%$. Larger water indices and smaller EWs are consistent with our [Fe/H] being smaller than those reported by Rojas-Ayala et al. (2012).

Although the spectral types of our stars fall within the range of the calibrations of Rojas-Ayala et al. (2012) and Terrien et al. (2012) (see § 3.2) there is one star (HIP 79431) with an [Fe/H] value outside the validity range of these two calibrations. In addition three others (GJ 179, GJ 436, and GJ 783.2 B) lie very close to the limits. Moreover, considering the results of Mann et al. (2013) and Terrien et al. (2015), the good agreement between our [Fe/H] values and those of Terrien et al. (2015) based on the K-band calibration of Mann et al. (2013), and that our spectra have similar resolution ($R \approx 1700$) to those used to built the Mann et al. (2013) calibrations, the following analyses are based exclusively on the K-band calibration of Mann et al. (2013).

4. PLANET-METALLICITY CORRELATION

4.1. *[Fe/H] for M Dwarfs with and without Planets*

As noted in § 1, the existence of a planet-metallicity correlation for M dwarfs has been strongly debated. In this section, we use the metallicities obtained from GNIRS data and the K-band calibration of Mann et al. (2013) to analyze the [Fe/H] of M stars with and without planets. Then, using relatively large and homogeneous samples from Terrien et al. (2015), we perform a similar analysis to verify that the trend found from our sample of 16 M-dwarf stars is consistent with the behaviour of larger samples.

Figure 6 shows the [Fe/H] distributions of our sample of stars with planets (SWP, N=11, red continuous line) and without planets (SWOP, N=5, black dash-line). The corresponding medians are: 0.25 and −0.25, respectively. The distributions are significantly different, according to the Kolmogorov-Smirnov (K-S, p-value = 0.05) test. This result suggests that M-dwarfs with planets are, on average, more metallic than those without planets. Table 4 summarizes the statistics.

To test if the trend found from GNIRS spectra is supported by a larger sample, we used the catalogue of Terrien et al. (2015) that provides homogeneous [Fe/H] values for 886 M dwarfs, based on the K-band calibration of Mann et al. (2013). These authors flagged 16 planet hosts in their sample. We identified two

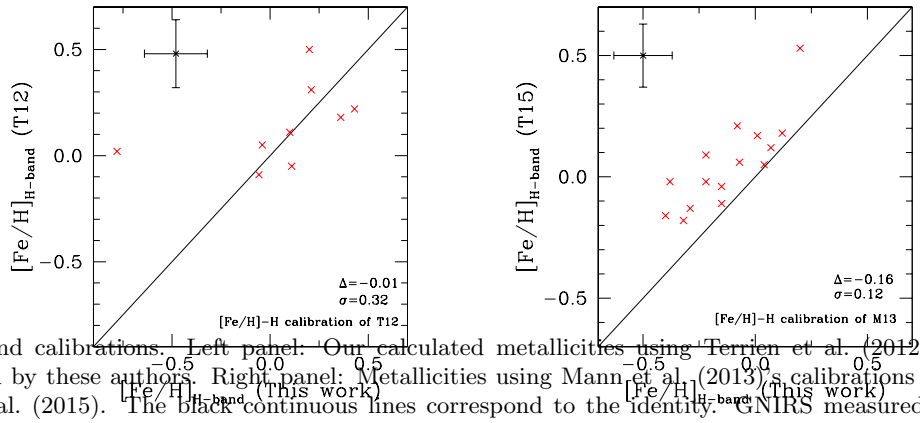

Fig. 5. *H*-band calibrations. Left panel: Our calculated metallicities using Terrien et al. (2012)'s calibrations vs. those reported by these authors. Right panel: Metallicities using Mann et al. (2013)'s calibrations vs. those reported in Terrien et al. (2015). The black continuous lines correspond to the identity. GNIRS measured [Fe/H] values are consistent with those of Terrien et al. (2012) within error bars, with exception of GJ 436, with relatively low SNR spectra. Our metallicities are in general ≈ 0.16 dex lower than those presented by Terrien et al. (2015).

TABLE 4

METALLICITY DISTRIBUTIONS OF THE SAMPLES OF M DWARFS WITH AND WITHOUT PLANET/S BUILT FROM GNIRS SPECTRA

Sample ID[1]	Number of stars	Average [Fe/H][2]	Median [Fe/H][2]	p-value (K-S)[3]
SWP	11	0.21	0.25	0.01
SWOP	5	−0.44	−0.25	

[1]Notation: SWP: M dwarfs hosting planet/s; SWOP: M dwarfs without detected planet (see text for more details).

[2]Based on [Fe/H] values derived using GNIRS spectra and the K-band calibration of Mann et al. (2013).

[3]Probability of being drawn from the same distribution as the control sample, according to the two-sided Kolmogorov-Smirnov (K-S) test.

additional stars with planets: GJ 176 (Forveille et al. 2009) and GJ 3323 (Astudillo-Defru et al. 2017). The 18 M dwarfs with planets along with their [Fe/H] values are listed in Table 5.

To construct a control sample of stars with no evidence of planetary companions, we cross-matched the remaining stars in Terrien et al. (2015) against samples of M dwarfs monitored with the HIRES (Rauscher & Marcy 2006) and HARPS (Bonfils et al. 2013) spectrographs, and selected all the stars without reported planets. In addition, we also included M dwarfs from the Terrien et al. (2015) catalogue with enough photometric measurements (usually more than ≈ 6500 data points) obtained with the *Kepler* space mission and/or the SuperWASP ground-based survey and with no detected planets. In this way, we built a final control sample of 213 M dwarfs that were searched for planets, but for which no planet has been reported so far. The selected M dwarfs without known planets along with the [Fe/H] values from the Terrien et al. (2015) catalogue are listed in Table 6. We caution, however, that this comparison sample might still include stars hosting low mass and/or long period planets that could be harder to detect by the mentioned surveys.

Figure 7 shows the normalised metallicity histograms along with the cumulative frequencies for the M dwarfs with planets (SWP, N=18, red continuous line) and without known planets (SWOP, N=213, black dashed line), based on *K*-band [Fe/H] values from Terrien et al. (2015). The sample of M dwarfs with planets has a median metallicity of +0.18 dex, whereas the control sample has a median of +0.05 dex. The two-sided K-S test gives a probability of 0.11 that both samples share the same parent distribution. Table 7 summarizes the statistics. The distribution of M dwarfs with planets is shifted toward higher metallicities with respect to the control

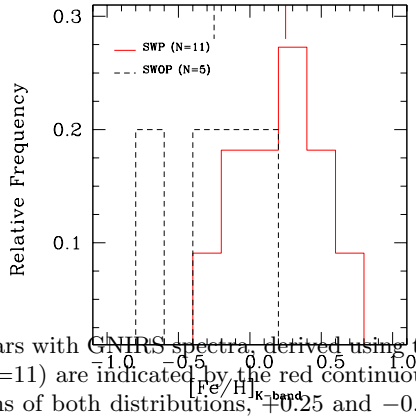

Fig. 6. Metallicity distributions for stars with GNIRS spectra, derived using the calibration of Mann et al. (2013) in the K band. Stars with planets (SWP, N=11) are indicated by the red continuous line and without planets (SWOP, N=5) by the black dashed line. The medians of both distributions, +0.25 and −0.25, are indicated. The color figure can be viewed online.

TABLE 5

[Fe/H] OF KNOWN M-DWARF-PLANET HOSTS FROM THE TERRIEN ET AL. (2015) CATALOGUE

Name	[Fe/H]	Planet type†
GJ 1214	0.40	super-Earth
GJ 176	0.23	super-Earth
GJ 179	0.25	Jupiter
GJ 317	0.43	2 Jupiters
GJ 436	0.00	Neptune
GJ 581	−0.02	Neptune + 2 super-Earths
GJ 649	0.04	Jupiter + super-Earth
GJ 849	0.50	2 Jupiters
GJ 876	0.31	2 Jupiters + Neptune + super-Earth
HIP 57050	0.04	Jupiter
HIP 79431	0.78	Jupiter
WASP 43	0.40	Jupiter
GJ 433	−0.03	Jupiter + super-Earth
WASP 80	0.13	Jupiter
GJ 15 A	−0.28	super-Earth
GJ 3323	−0.06	2 super-Earths
GJ 3470	0.27	Neptune
Kepler 138	−0.21	2 Earths + Mars

†Classification derived from masses (and/or radii) reported in The Extrasolar Planets Encyclopaedia (available at `www.exoplanet.eu`).

sample by ≈ 0.11 dex, showing the same trend found from the sample based on GNIRS data. This result is in agreement with the planet-metallitic correlation for M dwarfs with planets found by other authors (e.g. Johnson & Apps 2009, Rojas-Ayala et al. 2010, Terrien et al. 2012, Neves et al. 2013, Gaidos & Mann 2014) and it is also consistent with the metallicity enhancement found in solar-type stars with planets (e.g. Fischer & Valenti 2005, Santos et al. 2004, Santos et al. 2005, Ghezzi et al. 2010b, Maldonado et al. 2013).

TABLE 6

CONTROL SAMPLE WITHOUT KNOWN PLANETS AND K-BAND [Fe/H] FROM TERRIEN ET AL. CATALOGUE

Star	[Fe/H]	Star	[Fe/H]
2MASSJ02361535+0652191	−0.29	2MASSJ12241121+2653166	−0.13
2MASSJ03132299+0446293	0.24	2MASSJ23465800+2750066	0.12
2MASSJ04425581+1857285	0.23	2MASSJ12214070+2707510	−0.1 0
2MASSJ05015746−0656459	−0.06	2MASSJ23461405+2826036	−0.05
2MASSJ06521804−0511241	−0.09	2MASSJ00580115+3919111	−0.03
2MASSJ10121768−0344441	0.17	2MASSJ00270673+4941531	0.25
2MASSJ10285555+0050275	−0.19	2MASSJ09301445+2630250	0.22
2MASSJ10505201+0648292	0.29	2MASSJ02564122+3522346	0.24
2MASSJ11474440+0048164	−0.08	2MASSJ01270042+3351580	0.33
2MASSJ13295979+1022376	−0.12	2MASSJ13345147+3746195	0.21
2MASSJ14341683−1231106	0.42	2MASSJ04310001+3647548	0.12
2MASSJ15192689−0743200	−0.02	2MASSJ15512179+2931062	−0.11
2MASSJ17574849+0441405	−0.41	2MASSJ03302331+3440325	0.09
2MASSJ18050755−0301523	−0.26	2MASSJ21012481+2043377	−0.15
2MASSJ18424498+1354168	0.14	2MASSJ12362870+3512007	0.10
2MASSJ19095098+1740074	0.07	2MASSJ15493833+3448555	0.34
2MASSJ19220206+0702310	−0.28	2MASSJ02591670+3146245	0.01
2MASSJ20403364+1529572	0.33	2MASSJ20260528+5834224	0.30
2MASSJ22094029−0438267	0.50	2MASSJ12130291+2146388	−0.35
2MASSJ22531672−1415489	0.31	2MASSJ16061363+2901553	0.51
2MASSJ22563497+1633130	0.37	2MASSJ23435310+3235388	0.03
2MASSJ00182549+4401376	−0.1	2MASSJ17373648+2205510	0.08
2MASSJ02001278+1303112	−0.15	2MASSJ03360868+3118398	−0.04
2MASSJ02361535+0652191	−0.29	2MASSJ10361794+2844471	−0.18
2MASSJ06521804−0511241	−0.09	2MASSJ23442084+2136050	0.28
2MASSJ08524084+2818589	0.49	2MASSJ02000280+4345286	−0.09
2MASSJ10121768−0344441	0.17	2MASSJ10350859+3349499	−0.04
2MASSJ10285555+0050275	−0.19	2MASSJ02000280+4345286	−0.09
2MASSJ10505201+0648292	0.29	2MASSJ23385568+2101218	0.11
2MASSJ11474440+0048164	−0.08	2MASSJ23071524−2307533	−0.06
2MASSJ13295979+1022376	−0.12	2MASSJ22225080+2801475	0.22
2MASSJ14341683−1231106	0.42	2MASSJ02132062+3648506	−0.05
2MASSJ17574849+0441405	−0.41	2MASSJ15383708+3707247	0.01
2MASSJ18050755−0301523	−0.26	2MASSJ11263757+3756237	0.15
2MASSJ18343664+4007266	0.84	2MASSJ03564330+3254082	0.07
2MASSJ22464980+4420030	0.05	2MASSJ18562628+4622532	−0.01
2MASSJ22563497+1633130	0.37	2MASSJ03323578+2843554	−0.19
2MASSJ23415498+4410407	0.55	2MASSJ13455527+2723131	0.18
2MASSJ18550451+4259510	0.11	2MASSJ03323578+2843554	−0.19
2MASSJ19051335+3845050	0.06	2MASSJ23450868+3003184	−0.15
2MASSJ19051739+4507161	−0.19	2MASSJ18523373+4538317	−0.04
2MASSJ19170558+4007235	−0.19	2MASSJ11281625+3136017	0.20
2MASSJ19242100+4237254	0.44	2MASSJ13514938+4157445	0.39
2MASSJ19271753+4231537	−0.07	2MASSJ13505181+3644168	−0.07
2MASSJ19510930+4628598	−0.05	2MASSJ11353198+3855372	0.08
2MASSJ17283039+3727074	−0.09	2MASSJ12242665+2545077	−0.06
2MASSJ17074035+4918351	0.01	2MASSJ16041322+2331386	0.13
2MASSJ17340562+4447082	0.23	2MASSJ11240434+3808108	0.00
2MASSJ17363485+4549324	0.40	2MASSJ02224082+3055161	−0.03
2MASSJ16352740+3500577	−0.06	2MASSJ10331367+3409120	−0.15
2MASSJ17302672+3344522	0.26	2MASSJ22182135+4356406	−0.15
2MASSJ17173857+5224227	−0.01	2MASSJ01401649+3147306	0.25
2MASSJ17032384+5124219	0.03	2MASSJ10335971+2922465	0.03
2MASSJ16454410+3605496	−0.22	2MASSJ00252063+2253121	−0.01
2MASSJ17092601+3909384	−0.2	2MASSJ00243478+3002295	0.23
2MASSJ17080710+4829268	−0.02	2MASSJ21395433+2736439	−0.25
2MASSJ17072670+3900429	0.11	2MASSJ20592035+5303049	0.13
2MASSJ17101101+4139340	0.11	2MASSJ17195948+2412054	0.10
2MASSJ23225835+3717143	−0.10	2MASSJ17190577+2253036	0.35
2MASSJ17101101+4139340	0.11	2MASSJ00285391+5022330	0.15

TABLE 6 (CONTINUED)

Star	[Fe/H]	Star	[Fe/H]
2MASSJ22294885+4128479	−0.02	2MASSJ13093495+2859065	0.02
2MASSJ16495034+4745402	0.16	2MASSJ05030563+2122362	0.07
2MASSJ16480454+4522429	0.09	2MASSJ12462672+2626368	0.08
2MASSJ15315427+2851096	0.19	2MASSJ12503457+2655230	−0.1
2MASSJ16533915+5603272	−0.22	2MASSJ04342248+4302148	0.22
2MASSJ16312806+4710212	0.04	2MASSJ13220965+4144432	−0.12
2MASSJ02000741+3639481	0.10	2MASSJ14170294+3142472	0.10
2MASSJ12265737+2700536	0.11	2MASSJ07003840+3334581	0.16
2MASSJ23292258+4127522	0.24	2MASSJ00383388+5127579	−0.17
2MASSJ16342040+5709439	−0.4	2MASSJ16505794+2227058	−0.16
2MASSJ12255421+2651387	−0.07	2MASSJ00383388+5127579	−0.17
2MASSJ22011310+2818248	0.02	2MASSJ03563308+3157248	0.21
2MASSJ18352722+4545403	−0.17	2MASSJ16541912+2537363	−0.14
2MASSJ16495777+4601418	0.10	2MASSJ04040615+3042454	−0.39
2MASSJ23384176+3909262	0.08	2MASSJ16541912+2537363	−0.14
2MASSJ17555802+2926097	0.15	2MASSJ23215594+2412321	0.12
2MASSJ22172586+2335047	0.04	2MASSJ23495384+2721406	0.02
2MASSJ12250262+2642382	0.04	2MASSJ19071270+4416070	0.31
2MASSJ17393223+2746366	0.08	2MASSJ22384426+2513305	0.08
2MASSJ13314666+2916368	0.12	2MASSJ08175130+3107455	0.27
2MASSJ11315396+2725336	0.73	2MASSJ01382392+4516549	−0.24
2MASSJ13323908+3059065	0.17	2MASSJ00115302+2259047	0.25
2MASSJ18180345+3846359	−0.15	2MASSJ01040580+3938159	0.06
2MASSJ22232904+3227334	0.12	2MASSJ15294392+4252498	0.03
2MASSJ02591060+3636402	−0.01	2MASSJ05295269+3204524	−0.25
2MASSJ23575452+2159281	0.23	2MASSJ12232063+2529441	0.15
2MASSJ16071362+2650173	−0.2	2MASSJ09370355+4034389	0.15
2MASSJ13332256+3620352	0.37	2MASSJ23454076+4942300	0.23
2MASSJ17002033+2521028	−0.18	2MASSJ08155393+3136392	0.28
2MASSJ00085391+2050252	0.15	2MASSJ09093060+3249091	−0.22
2MASSJ12305549+3152121	0.16	2MASSJ21362954+5331585	0.14
2MASSJ13451104+2852012	−0.11	2MASSJ12424996+4153469	0.30
2MASSJ23295502+2211442	−0.36	2MASSJ23454076+4942300	0.23
2MASSJ12292712+2259467	0.00	2MASSJ21362954+5331585	0.14
2MASSJ21395433+2736439	−0.25	2MASSJ23454076+4942300	0.23
2MASSJ21415843+2741150	−0.20	2MASSJ10145315+2123464	0.07
2MASSJ21395433+2736439	−0.25	2MASSJ01512417+2123399	0.17
2MASSJ21415843+2741150	−0.2	2MASSJ21274751+5505337	−0.21
2MASSJ01031395+3140598	0.30	2MASSJ21462206+3813047	−0.56
2MASSJ14412571+2839269	0.28	2MASSJ19562490+5909216	−0.44
2MASSJ23422211+3458276	0.12	2MASSJ02085359+4926565	0.13
2MASSJ23545147+3831363	0.14	2MASSJ06222070+3326564	0.39
2MASSJ12573935+3513194	−0.08	2MASSJ10494561+3532515	−0.49
2MASSJ16043696+2620430	−0.01	2MASSJ21462206+3813047	−0.56
2MASSJ23425274+3049219	0.05	2MASSJ23565510+2305033	−0.07
2MASSJ23423350+3914234	−0.39	2MASSJ01431186+2101106	0.33
2MASSJ23505402+3829334	0.39		

4.2. *Metallicity vs. Planetary Parameters*

To investigate whether the correlations between [Fe/H] and planetary parameters found for FGK main-sequence stars (e.g. Fischer & Valenti 2005, Buchhave et al. 2012, Adibekyan et al. 2013) are valid for M-type stars we searched for correlations of [Fe/H] with planetary masses planet types, orbital periods, and eccentricities. For this analysis, we first used the 11 stars with planets observed with GNIRS and then the 18 stars with planets (which also include the stars with planets observed with GNIRS) and the control sample derived from Terrien et al. (2015) catalogue (see Table 6). Planetary parameters (masses, periods, and eccentricities) were obtained from The Extrasolar Planets Encyclopaedia.

4.2.1. *Metallicity vs M-Dwarfs hosting Jovian-Mass and Lower-Mass Planets*

We constructed two sub-samples from the 11 M-dwarf stars with planets (SWP) observed with GNIRS: stars with at least one Jupiter-mass planet (SWJP) and those hosting only lower mass planets ($M_p \sin i < 25 M_\oplus$,

TABLE 7

METALLICITY DISTRIBUTIONS OF M DWARFS WITH PLANET/S AND THE CONTROL SAMPLE BUILT FROM TERRIEN ET AL.'S CATALOGUE

Sample ID[1]	Number of stars	Average [Fe/H][2]	Median [Fe/H][2]	p-value (K-S)[3]
SWP	18	0.18	0.18	0.11
SWOP	213	0.04	0.05	

[1]Notation: SWP: M dwarfs hosting planet/s; SWOP: control sample without detected planets (see text for more details).

[2]Based on [Fe/H] values derived by Terrien et al. (2015) using the K-band calibration of Mann et al. (2013).

[3]Probability of being drawn from the same distribution as the control sample, according to the two-sided Kolmogorov-Smirnov (K-S) test.

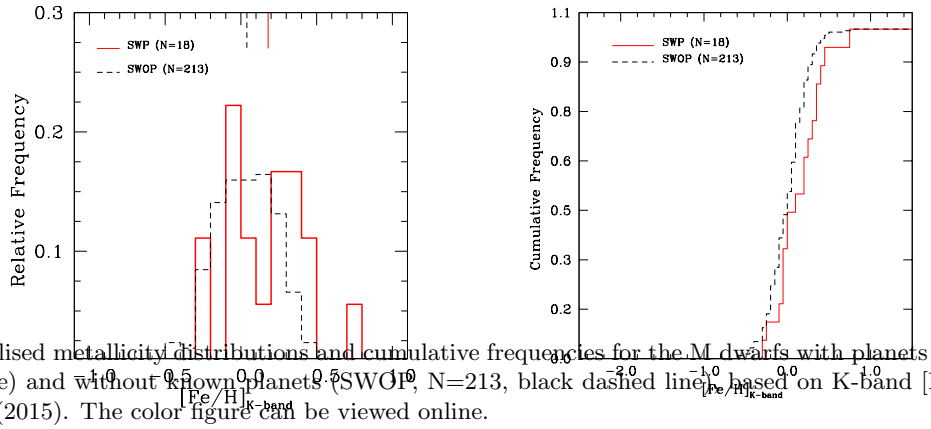

Fig. 7. Normalised metallicity distributions and cumulative frequencies for the M dwarfs with planets (SWP, N=18, red continuous line) and without known planets (SWOP, N=213, black dashed line), based on K-band [Fe/H] values from Terrien et al. (2015). The color figure can be viewed online.

mainly Neptune- and super-Earth mass planets, SWLP). In a similar manner, we classified the sample of 18 M-dwarf stars with planets from Terrien et al. (2015) in two sub-sets.

Figure 8 shows the cumulative frequency distributions for Jupiter-like hosts (blue continuous line), low-mass (Neptune and super-Earth type) planets (red continuous line) in comparison with the control sample (black dashed line) from the Terrien et al. (2015) catalogue. The left panel corresponds to the GNIRS sample, the right panel to the Terrien et al. (2015) sub-set. Table 8 summarizes the statistics for both samples. We note that both samples of stars with planets are compared with the Terrien et al. (2015) control sample. We observed only 5 stars without planets with GNIRS (see Table 1). However the trend in Table 8 for GNIRS stars with planets remains, even if such a small control sample is used.

The K-S test gives p-values of 0.02 and 0.01 (GNIRS and Terrien et al. (2015)'s samples, respectively) that the hosts of giant planets and the M-dwarf control sample are drawn from the same parent distribution. The metallicity distributions of Jupiter-like hosts are clearly shifted, by $\approx +0.20$ dex, to higher metallicities compared with the control sample, for both GNIRS and Terrien et al. (2015) samples. On the other hand, the [Fe/H] distributions of stars hosting low-mass planets and those without known planets are very similar. In this case, the K-S test gives p-values of 0.97 and 0.75 (GNIRS and Terrien et al. (2015)'s samples) that Neptune and super-Earth hosts share the same metallicity distribution as the control sample.

It must be noted, however, that the orbital inclinations of the planets - and hence the true masses - have only been determined for a third of the planets under consideration. For the remaining planets, only the lower bound of $M \sin(i)$ is known. In addition we caution about the small number of objects in both sub-samples with planets and the need to increase the number of M dwarfs with planets to put this initial result on more

TABLE 8

METALLICITY DISTRIBUTIONS OF DIFFERENT M-DWARF SAMPLES WITH GIANT AND LOW-MASS PLANETS

Sample ID[1]	Number of stars	Average [Fe/H][2]	Median [Fe/H][2]	p-value (K-S)[3]
		GNIRS sample		
SWJP	7	0.28	0.26	0.02
SWLP	4	0.07	0.05	0.97
		Terrien et al. (2015)'s catalogue		
SWJP	10	0.30	0.28	0.01
SWLP	8	0.02	−0.01	0.75

[1]Notation: SWJP: M dwarfs harbouring at least one giant planet; SWLP: M dwarfs hosting only low-mass planets.

[2]Based on [Fe/H] values derived using the K-band calibration of Mann et al. (2013).

[3]Probability of being drawn from the same distribution as the control sample, according to the two-sided Kolmogorov-Smirnov (K-S) test.

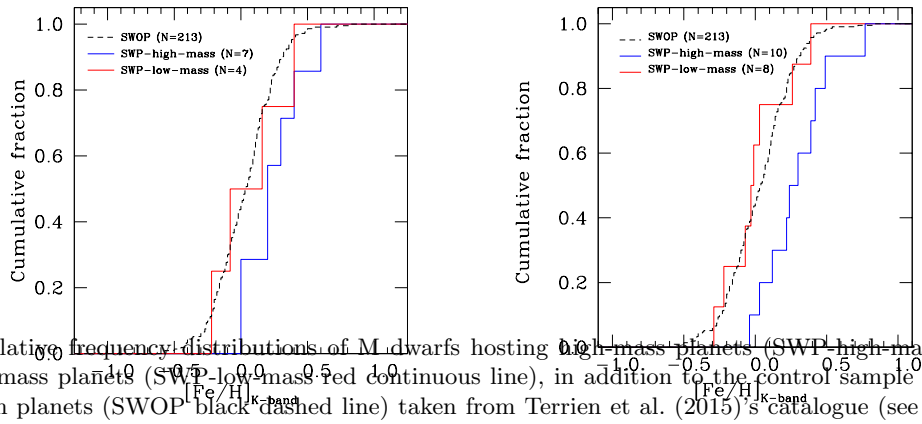

Fig. 8. Cumulative frequency distributions of M dwarfs hosting high-mass planets (SWP-high-mass blue continuous line) and low-mass planets (SWP-low-mass red continuous line), in addition to the control sample composed by stars without known planets (SWOP black dashed line) taken from Terrien et al. (2015)'s catalogue (see Table 6). The left panel shows only the metallicties derived from GNIRS spectra, except for the control sample. The right panel shows metallicities from Terrien et al. (2015). The color figure can be viewed online.

solid grounds. On the other hand, we note that in spite of the small numbers of M-dwarfs with planets, GNIRS based samples agree with Terrien et al. (2015).

This analysis suggests that, like their more massive solar-type counterparts (Sousa et al. 2008, Ghezzi et al. 2010b, Mayor et al. 2011, Buchhave et al. 2012, Neves et al. 2013), M dwarfs hosting low-mass planets are not preferentially metal-rich. In addition, this result is in line with similar suggestions obtained from smaller samples of M dwarfs with planets (Johnson & Apps 2009, Rojas-Ayala et al. 2012, Terrien et al. 2012, Gaidos & Mann 2014).

The apparent separation in metallicity between host stars harboring only Neptune and/or super-Earth type planets and those with at least one Jupiter-type planet can be explained in the context of the core accretion model of planetary formation. This model postulates that only metal-rich disks would form cores rapidly enough to allow for gas accretion on a scale sufficient to form Jupiter-type planets before the gas dissipates, as described in § 1.

4.2.2. *Metallicity vs Planetary Periods and Eccentricities*

Figure 9 shows planetary periods (left panels) and eccentricities (right panels) vs. metallicity for the 11 M-dwarfs observed with GNIRS (upper panels) and the 18 M-dwarfs with planets in the Terrien et al. (2015) catalogue (lower panels). The orbital period does not show any significant correlation with stellar metallicity. For FGK stars, Fischer & Valenti (2005) also found no correlation between orbital period and stellar metallicity. However, Adibekyan et al. (2013) found that planets orbiting metal-poor FGK stars have longer periods than those orbiting metal-rich stars; they explain this by assuming that planets formed in metal-poor disks form farther out and/or later and so do not migrate as far in as those from metal-rich disks. While the apparent lack of such a differentiation may hint at different migration scenarios for planets around M-dwarfs to those around FGK stars, the low number of objects analysed here in comparison with those analysed by Adibekyan et al. (2013) means this must be treated with caution. The eccentricity does not show any apparent correlation with stellar metallicity, as can be seen in Figure 9, right panels. This is consistent with both Fischer & Valenti's (2005) and Adibekyan et al.'s (2013) results for FGK stars, although, again, we should caution about the relatively small number of objects analysed.

Finally, it is fair to caution that multiple factors such as stellar temperature may affect metallicity determinations, particularly for late spectral type stars. As discussed in the previous sections, on average, M-dwarfs with planets are metal-rich with respect to M-dwarfs without known planets, providing support to the core accretion model. However, the metallicity excess is only about 0.10 dex, i.e., not large enough to safely ignore any bias or uncertainty in the determinations. In the same sense, correlations (or lack thereof) with planetary parameters should be taken under the caveat of effects that may compromise metallicity determinations available today, as well as the relatively small sample of M-dwarfs with planets.

5. SUMMARY AND CONCLUSIONS

In this work, we have determined the effective temperature, radius, luminosity, and metallicity for a sample of 16 M-dwarf stars (including 11 with planets), using NIR spectra obtained with the GNIRS instrument on the Gemini North telescope. Metallicities were derived using the calibrations defined by Rojas-Ayala et al. (2012), Terrien et al. (2012), and Mann et al. (2013) whilst the remaining stellar parameters were determined employing the calibrations of Newton et al. (2015). In general, for all the parameters we found a good agreement, (within error bars) between our values and other determinations from the literature; in this way, we have shown that GNIRS spectra can be used for the determination of reliable stellar parameters for M-dwarf stars, and in particular of metallicities.

We adopted metallicities obtained from the K-band Mann et al. (2013)'s calibration and compared the distributions of metallicities of M-dwarfs with and without known planets in our sample. The distributions are significantly different, with stars with planets being more metallic than those without planets. This result is supported by the analysis of a larger sample of M-dwarfs with planets (18 stars) and without known planets (213 stars) obtained from the catalogue of Terrien et al. (2015).

We searched for correlations between the planetary masses, periods and eccentricities and the metallicities, using our GNIRS sample of 11 M dwarfs with planet/s and the relatively larger sample (18 objects) of Terrien et al. (2015). The results coincide, confirming the initial trend derived from GNIRS spectra. We found that the sub-sample of M dwarfs with at least one Jupiter-mass planet is more metal-rich than the sub-sample with Neptune or super-Earth planets. The latter sample is also indistinguishable from the control field. More metallic stars host larger (giant) planets. However, it must be noted that for two-thirds of the planets, only the lower bound of $M \sin(i)$ is known, not the actual mass. The planet-metallicity correlation as well as the trend of more metallic stars to host giant planets support the core accretion model of planetary formation.

In summary, our results suggest that M dwarfs hosting planets follow the planet-metallicity correlation already observed for FGK stars, as well as the trend of more metallic stars to host giant planets. In addition, our analyses show the utility of GNIRS spectra to derive reliable stellar parameters for M dwarfs. In the future, we expect to increase the initial observed sample in order to confirm, with higher statistical significance and in a homogeneous way, the planet-metallicity correlation of M dwarfs with planets and the trend of giant planets to preferentially occur around metal-rich stars.

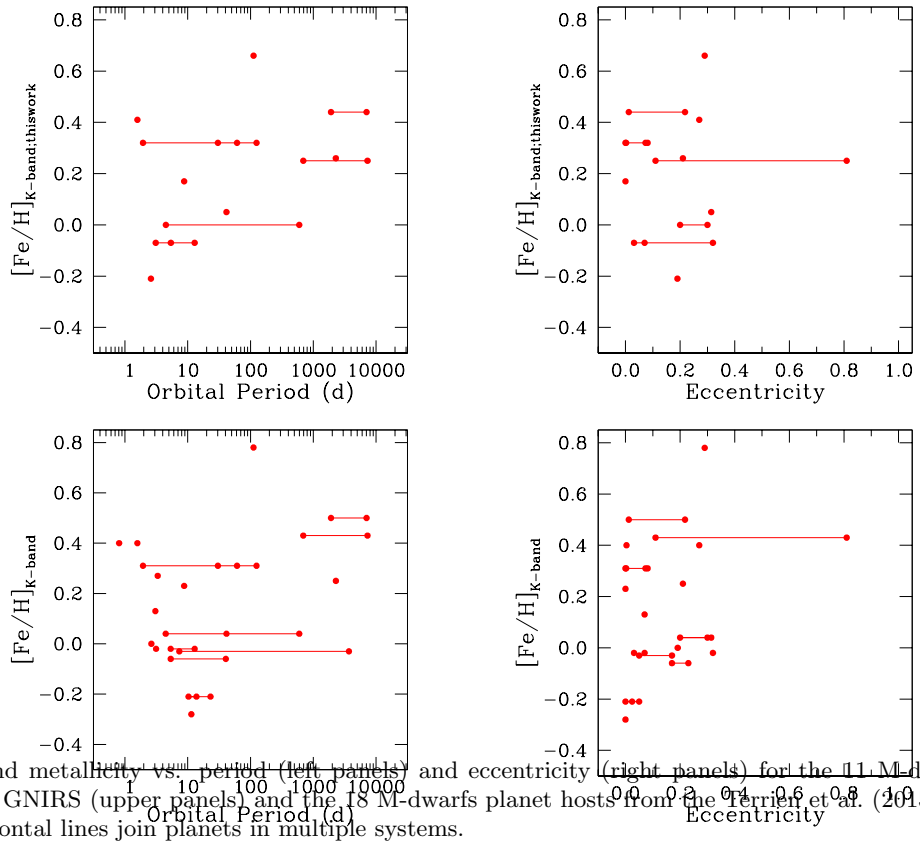

Fig. 9. K-band metallicity vs. period (left panels) and eccentricity (right panels) for the 11 M-dwarfs with planets observed with GNIRS (upper panels) and the 18 M-dwarfs planet hosts from the Terrien et al. (2015) catalogue (lower panels). Horizontal lines join planets in multiple systems.

Based on observations obtained at the Gemini Observatory, which is operated by the Association of Universities for Research in Astronomy, Inc., under a cooperative agreement with the NSF on behalf of the Gemini partnership: the National Science Foundation (United States), the National Research Council (Canada), CONICYT (Chile), Ministerio de Ciencia, Tecnología e Innovación Productiva (Argentina), and Ministério da Ciência, Tecnologia e Inovação (Brazil). This research has made use of the SIMBAD database, operated at CDS, Strasbourg, France. We gratefully acknowledge financial support from CONICET (Consejo Nacional de Investigaciones Científicas y Técnicas, Argentina) through grant PIP CONICET No. 11220120100497. E.J. and R.P. acknowledge the financial support from CONICET in the form of Post-Doctoral Fellowships. We thank Rachel Mason and Omaira González-Martín for making their data reduction pipeline publicly available. We also thank the referee for constructive comments and suggestions that greatly improved the paper.

REFERENCES

Adibekyan, V. Z., Figueira, P., Santos, N. C., et al. 2013, A&A, 560, A51
Apps, K., Clubb, K. I., Fischer, D. A., et al. 2010, PASP, 122, 156
Astudillo-Defru, N., Forveille, T., Bonfils, X., et al. 2017, A&A, 602, A88
Bean, J. L., Benedict, G. F., & Endl, M. 2006, ApJ, 653, L65
Bonfils, X., Delfosse, X., Udry, S., et al. 2013, A&A, 549, A109
Bonfils, X., Delfosse, X., Udry, S., et al. 2005a, A&A, 442, 635
Bonfils, X., Forveille, T., Delfosse, X., et al. 2005b, A&A, 443, L15
Boss, A. P. 1997, BAAS, 29, 1254
Buchhave, L. A. & Latham, D. W. 2015, ApJ, 808, 187

Buchhave, L. A., Latham, D. W., Johansen, A., et al. 2012, Natur, 486, 375
Butler, R. P., Johnson, J. A., Marcy, G. W., Wright, J. T., Vogt, S. S., & Fischer, D. A. 2006, PASP, 118, 1685
Butler, R. P., Vogt, S. S., Marcy, G. W., et al. 2004, ApJ, 617, 580
Charbonneau, D., Berta, Z. K., Irwin, J., et al. 2009, Natur, 462, 891
Delfosse, X., Forveille, T., Mayor, M., et al. 1998, A&A, 338, L67
Endl, M., Cochran, W. D., Wittenmyer, R. A., & Boss, A. P. 2008, ApJ, 673, 1165
Fischer, D. A. & Valenti, J. 2005, ApJ, 622, 1102
Forveille, T., Bonfils, X., Delfosse, X., et al. 2009, A&A, 493, 645
Gaia Collaboration, Prusti, T., de Bruijne, J. H. J., Brown, A. G. A., et al. 2016, A&A, 595, A1
Gaidos, E. & Mann, A. W. 2014, ApJ, 791, 54
Gaidos, E., Mann, A. W., Kraus, A. L., & Ireland, M. 2016, MNRAS, 457, 2877
Ghezzi, L., Cunha, K., Schuler, S. C., & Smith, V. V. 2010a, ApJ, 725, 721
Ghezzi, L., Cunha, K., Smith, V. V., et al. 2010b, ApJ, 720, 1290
Ghezzi, L. & Johnson, J. A. 2015, ApJ, 812, 96
Goldreich, P. & Ward, W. R. 1973, ApJ, 183, 1051
Gonzalez, G. 1997, MNRAS, 285, 403
Haghighipour, N., Vogt, S. S., Butler, R. P., et al. 2010, ApJ, 715, 271
Howard, A. W., Johnson, J. A., Marcy, G. W., et al. 2010, ApJ, 721, 1467
Ida, S. & Lin, D. N. C. 2004, ApJ, 604, 388
Jofré, E., Petrucci, R., Saffe, C., et al. 2015, A&A, 574, A50
Johnson, J. A. & Apps, K. 2009, ApJ, 699, 933
Johnson, J. A., Butler, R. P., Marcy, G. W., et al. 2007, ApJ, 670, 833
Johnson, J. A., Howard, A. W., Marcy, G. W., et al. 2010, PASP, 122, 149
Johnson, J. L. & Li, H. 2012, ApJ, 751, 81
Kaltenegger, L. & Traub, W. A. 2009, ApJ, 698, 519
Kroupa, P., Weidner, C., Pflamm-Altenburg, J., et al. 2013, The Stellar and Sub-Stellar Initial Mass Function of Simple and Composite Populations, (Dordrecht: Springer)
Lada, C. J. 2006, ApJ, 640, L63
Laughlin, G., Bodenheimer, P., & Adams, F. C. 2004, ApJ, 612, L73
Maldonado, J., Villaver, E., & Eiroa, C. 2013, A&A, 554, A84
Mann, A. W., Brewer, J. M., Gaidos, E., Lépine, S., & Hilton, E. J. 2013, AJ, 145, 52
Mann, A. W., Deacon, N. R., Gaidos, E., et al. 2014, AJ, 147, 160
Mann, A. W., Feiden, G. A., Gaidos, E., Boyajian, T., & von Braun, K. 2015, ApJ, 804, 64
Marcy, G. W., Butler, R. P., Fischer, D., et al. 2001, ApJ, 556, 296
Mayor, M., Bonfils, X., Forveille, T., et al. 2009, A&A, 507, 487
Mayor, M., Marmier, M., Lovis, C., et al. 2011, arXiv:1109.2497
Montet, B. T., Crepp, J. R., Johnson, J. A., Howard, A. W., & Marcy, G. W. 2014, ApJ, 781, 2B
Mordasini, C., Alibert, Y., & Benz, W. 2009, A&A, 501, 1139
Mordasini, C., Alibert, Y., Benz, W., Klahr, H., & Henning, T. 2012, A&A, 541, A97
Muirhead, P. S., Becker, J., Feiden, G. A., et al. 2014, ApJS, 213, 5
Neves, V., Bonfils, X., Santos, N. C., et al. 2013, A&A, 551, A36
Newton, E. R., Charbonneau, D., Irwin, J., et al. 2014, AJ, 147, 20
Newton, E. R., Charbonneau, D., Irwin, J., & Mann, A. W. 2015, ApJ, 800, 85
Niedzielski, A., Konacki, M., Wolszczan, A., et al. 2007, ApJ, 669, 1354
Önehag, A., Heiter, U., Gustafsson, B., et al. 2012, A&A, 542, A33
Pollack, J. B., Hubickyj, O., Bodenheimer, P., et al. 1996, Icarus, 124, 62
Rauscher, E. & Marcy, G. W. 2006, PASP, 118, 617
Reffert, S., Bergmann, C., Quirrenbach, A., Trifonov, T., & Künstler, A. 2015, A&A, 574, A116
Rivera, E. J., Laughlin, G., Butler, R. P., et al. 2010, ApJ, 719, 890
Rivera, E. J., Lissauer, J. J., Butler, R. P., et al. 2005, ApJ, 634, 625
Rojas-Ayala, B., Covey, K. R., Muirhead, P. S., & Lloyd, J. P. 2010, ApJ, 720, L113
_____. 2012, ApJ, 748, 93
Santos, N. C., Bouchy, F., Mayor, M., et al. 2004, A&A, 426, L19
Santos, N. C., Israelian, G., Mayor, M., et al. 2005, A&A, 437, 1127
Santos, N. C., Mayor, M., Benz, W., et al. 2010, A&A, 512, A47
Sato, B., Kambe, E., Takeda, Y., et al. 2005, PASJ, 57, 97
Schlaufman, K. C. & Laughlin, G. 2010, A&A, 519, A105
Sembach, K. R. & Savage, B. D. 1992, ApJS, 83, 147
Sousa, S. G., Santos, N. C., Israelian, G., Mayor, M., & Udry, S. 2011, A&A, 533, A141
Sousa, S. G., Santos, N. C., Mayor, M., et al. 2008, A&A, 487, 373
Souto, D., Cunha, K., García-Hernández, D. A., et al. 2017, ApJ, 835, 239
Terrien, R. C., Mahadevan, S., Bender, C. F., et al. 2012, ApJ, 747, L38
Terrien, R. C., Mahadevan, S., Deshpande, R., & Bender, C. F. 2015, ApJS, 220, 16
Udry, S., Bonfils, X., Delfosse, X., et al. 2007, A&A, 469, L43
Wang, J. & Fischer, D. A. 2015, AJ, 149, 14
Wenger, M., Ochsenbein, F., Egret, D., et al. 2000, A&AS, 143, 9

Wittenmyer, R. A., Wang, S., Horner, J., et al. 2013, ApJS, 208, 2
Woolf, V. M. & Wallerstein, G. 2006, PASP, 118, 218
Youdin, A. N. & Shu, F. H. 2002, ApJ, 580, 494

L. García, M. Gómez, M. J. Hobson, E. Jofré, and R. Petrucci: Observatorio Astronómico de Córdoba, Laprida 854, Córdoba, Argentina (melissa.hobson@lam.fr).
M. Gómez, E. Jofré, and R. Petrucci: Consejo Nacional de Investigaciones Científicas y Técnicas (CONICET), Argentina.